Carbohydrate Polymers 114 (2014) 407–415

Contents lists available at ScienceDirect

Carbohydrate Polymers

journal homepage: www.elsevier.com/locate/carbpol

Hyaluronic acid-coated solid lipid nanoparticles for targeted delivery of vorinostat to CD44 overexpressing cancer cells

Tuan Hiep Tran[a], Ju Yeon Choi[a], Thiruganesh Ramasamy[a], Duy Hieu Truong[a], Chien Ngoc Nguyen[b], Han-Gon Choi[c], Chul Soon Yong[a,**], Jong Oh Kim[a,*]

[a] College of Pharmacy, Yeungnam University, 214-1, Dae-Dong, Gyeongsan 712-749, South Korea
[b] National Institute of Pharmaceutical Technology, Hanoi University of Pharmacy, 13-15 Le Thanh Tong, Hoan Kiem, Ha Noi, Viet Nam
[c] College of Pharmacy, Hanyang University, 55, Hanyangdaehak-ro, Sangnok-gu, Ansan 426-791, South Korea

ARTICLE INFO

Article history:
Received 18 June 2014
Received in revised form 4 August 2014
Accepted 5 August 2014
Available online 23 August 2014

Keywords:
Vorinostat
Solid lipid nanoparticles
Hyaluronic acid
Chemotherapy
Targeting

ABSTRACT

Hyaluronic acid (HA)-decorated solid lipid nanoparticles (SLNs) were developed for tumor-targeted delivery of vorinostat (VRS), a histone deacetylase inhibitor. HA, a naturally occurring polysaccharide, which specifically binds to the CD44 receptor, was coated on a cationic lipid core through electrostatic interaction. After the optimization process, HA-coated VRS-loaded SLNs (HA-VRS-SLNs) were spherical, core-shell nanoparticles, with small size (~100 nm), negative charge (~−9 mV), and narrow size distribution. In vitro release profile of HA-VRS-SLNs showed a typical bi-phasic pattern. In addition, the intracellular uptake of HA-VRS-SLNs was significantly enhanced in CD44 overexpressing cells, A549 and SCC-7 cells, but reduced when HA-VRS-SLNs were incubated with SCC-7 cells pretreated with HA or MCF-7 cells with low over-expressed CD44. Of particular importance, HA-VRS-SLNs were more cytotoxic than the free drug and VRS-SLNs in A549 and SCC-7 cells. In addition, HA shell provided longer blood circulation and reduced VRS clearance rate in rats, resulting in enhanced higher plasma concentration and bioavailability. These results clearly indicated the potential of the HA-functionalized lipid nanoparticle as a nano-sized drug formulation for chemotherapy.

1. Introduction

Vorinostat (VRS), a histone deacetylase inhibitor, has been approved by the FDA for treatment of cutaneous T-cell lymphoma (CTCL) (Cai et al., 2010; Choo, Ho & Lin, 2008). In clinical trials, it was used for a variety of hematopoietic and solid tumor indications (Bolden, Peart & Johnstone, 2006; Kelly et al., 2005). It can effectively induce cell cycle arrest, cell differentiation, and apoptosis (Marks & Breslow, 2007). Despite showing such chemotherapeutic promise, the clinical application of VRS has been restricted due to its poor aqueous solubility and low membrane permeability, belonging to class IV of the Biopharmaceutics Classification System (BCS) (Mohamed et al., 2012). In addition, VRS exhibited a short half-life of 40 min following intravenous (IV) administration. To overcome these problems, VRS has been incorporated into micelle nanocarriers (Mohamed et al., 2012), inclusion cyclodextrins (Cai et al., 2010), and silicon microstructures (Strobl, Nikkhah & Agah, 2010), however, the efficiency of therapy is still a major question.

Solid lipid nanoparticles (SLNs) are a suitable candidate for delivery of hydrophobic and hydrophilic anti-cancer drugs. Owing to their lipid core, SLNs are expected to show high drug loading capacity, overcome multidrug resistance (MDR), modulate release kinetics, improve the blood circulation time, and increase the overall therapeutic efficacy of anti-cancer drugs (Bhushan et al., 2012; Lee, Lim & Kim, 2007; Luan et al., 2014). In addition, surface modification of SLNs with targeting moiety enables these SLNs to increase their selectivity for cellular binding and internalization (Venishetty, Komuravelli, Kuncha, Sistla & Diwan, 2013). In particular, the frequent overexpression of the hyaluronic acid (HA) receptors CD44 and CD168 (RHAMM) on many types of tumors opens new avenues for targeting by the naturally-occurring high-molecular weight HA (Rivkin, Cohen, Koffler, Melikhov, Peer & Margalit, 2010; Sun, Benjaminsen, Almdal & Andresen, 2012).

Therefore, in this study, we developed HA-coated VRS-loaded SLNs (HA-VRS-SLNs) for tumor-targeted delivery. We hypothesize that this system will demonstrate the combined advantages of high drug loading capacity by using lipid core, long blood circulation resulting from the hydrophilic surface and improved delivery

* Corresponding author. Tel.: +82 53 810 2813; fax: +82 53 810 4654.
** Corresponding author. Tel.: +82 53 810 2812; fax: +82 53 810 4654.
E-mail addresses: csyong@yu.ac.kr (C.S. Yong), jongohkim@yu.ac.kr (J.O. Kim).

http://dx.doi.org/10.1016/j.carbpol.2014.08.026
0144-8617/

by selective target of HA. To validate that, we investigated at the molecular, cellular, and whole animal levels of organization. The optimized HA-VRS-SLNs were evaluated in terms of physicochemical, thermal analyses, and ultrastructure characterization. The targeting efficacy of the HA-VRS-SLNs to tumor cells was estimated by intracellular uptake through confocal fluorescence image as well as flow-cytometric analysis in different cancer cell lines; the activity of VRS of HA-VRS-SLNs was then confirmed via cytotoxicity study. VRS plasma concentration, retention time and $AUC_{0-\infty}$ in blood circulation were compared among free drug, VRS-SLNs, and HA-VRS-SLNs for the *in vivo* study.

2. Materials and methods

2.1. Materials

VRS was purchased from LC Laboratories (MA, USA). Compritol 888 ATO (Compritol) (powder state; melting point, 70 °C) was obtained from Gattefosse (Cedex, France). 3-(4,5-Dimethylthiazol-2-yl)-2,5-diphenyl-tetrazolium bromide (MTT) and didecyldimethyl ammonium bromide (DDAB) were purchased from Sigma (St. Louis, MO, USA). Soybean lecithin was purchased from Junsei Co. Ltd (Tokyo, Japan). Hyaluronic acid (3 kDa) was supplied by B&K Technology Group Co. Ltd. (China). NBD-PC was supplied by Avanti Polar Lipids, Inc., and Lyso TrackerRed was purchased from Thermo Fisher Scientific Inc. The squamous cell carcinoma (SCC-7), human breast adenocarcinoma (MCF-7), human lung adenocarcinoma epithelial (A549) cells were originally obtained from the Korean Cell Line Bank (Seoul, South Korea). All cell lines were cultured in RPMI 1640 containing 10% fetal bovine serum (FBS), 100 U/mL penicillin G sodium, and 100 μg/mL streptomycin sulfate (complete 1640 medium) and incubated at 37 °C in 5% CO_2 atmosphere. All the cells threats such as fungi, bacteria, and mycoplasma were checked before carrying out experiments. All other chemicals were of reagent grade and were used without further purification.

2.2. Preparation of HA-VRS-SLNs

HA-VRS-SLNs were prepared by the hot homogenization method using an emulsification-sonication technique (Tran et al., 2014a). Based on a preliminary analysis of potential lipids and surfactants (data not shown), Compritol 888 ATO, DDAB, lecithin, and Tween 80 were selected for preparation of SLNs. Briefly, the lipid phase was prepared by melting Compritol 888 ATO, DDAB, lecithin, and VRS at 10 °C above the lipid melting point to obtain a clear transparent solution. The aqueous phase was prepared by dissolving Tween 80 in distilled water and heating to the final temperature of the lipid phase. Next, hot aqueous phase was gently added dropwise into the lipid phase with constant stirring at 13,500 rpm in an Ultra Turrax® T-25 homogenizer (IKA®-Werke, Staufen, Germany) for 3 min. The resulting coarse emulsion was immediately sonicated using a high-intensity probe sonicator (Vibracell VCX130; Sonics, USA) at 80% amplitude for 10 min. The resulting suspension was then cooled in an ice bath. For preparation of HA-VRS-SLNs, 1 mL of VRS-SLNs dispersion was slowly added under gentle stirring to a HA solution. The various concentrations of HA were investigated in order to obtain the optimum formulation.

Trehalose (5%, w/v) was used as a cryoprotectant in the freeze-drying process. The resulting nanoparticle dispersions were poured into glass bottles and pre-frozen at −80 °C for 24 h; later, the samples were freeze-dried using a lyophilizer (FDA5518, IlShin, South Korea) at a temperature of −25 °C for 24 h. The lyophilized powders were collected for further experiments.

2.3. Characterization of HA-VRS-SLNs

2.3.1. Measurement of particle size and zeta potential

Particle sizes of VRS-SLNs and HA-VRS-SLNs were analyzed by the dynamic light scattering (DLS) technique using a Zetasizer Nano–Z (Malvern Instruments, Worcestershire, UK) at a fixed scattering angle of 90° and a temperature of 25 °C. Prior to the measurement, colloidal dispersions were adequately diluted with distilled water. DLS results are presented as *z*-average diameter, polydispersity index (PDI), and ζ-potential. The data were determined using the Nano DTS software (version 6.34) provided by the manufacturers. All measurements were performed in triplicate.

2.3.2. Morphological analysis

The VRS-SLNs and HA-VRS-SLNs were deposited onto the surface of a copper grid (mesh size of 300) coated with carbon. Using 2% phosphotungstic acid (w/v), negative staining was performed on the samples, followed by air-drying for 15 min. The stained grids were subsequently probed using transmission electron microscopy (TEM) (Hitachi H-7100, Japan) to visualize the morphology of nanoparticles.

2.3.3. Physical characterization

Differential scanning calorimetry (DSC) analysis were performed using a differential scanning calorimeter DSC-Q200 (TA Instruments, New Castle, DE, USA) for lipid, drug and optimized formulation. Briefly, 2–3 mg lyophilized sample was loaded in an aluminum pan and then heated over the temperature range of 40–200 °C with the heating rate of 10 °C/min under nitrogen gas flow of 50 mL/min. An empty pan was used as a reference. The XRD patterns of the above mentioned samples were obtained using an X-ray diffractometer (X'Pert PRO MPD diffractometer, Almelo, The Netherlands) using Cu K_α radiation under voltage of 40 kV and current of 30 mA with a scan step size of 0.02.

2.4. Drug entrapment efficiency and drug loading capacity

The drug entrapment efficiency (EE) and drug loading capacity (LC) of VRS-SLNs and HA-VRS-SLNs were determined by measuring the amount of free drug in the dispersion medium. Ultrafiltration was performed on the VRS-SLNs and HA-VRS-SLNs using centrifugal 10-kDa molecular weight cut-off devices (Amicon Ultra, Millipore, USA). 2 mL of formulations was dispensed onto the top compartment of the devices, followed by centrifuging at 5000 rpm for 10 min. The filtrate was collected and diluted with acetonitrile at a ratio of 1:1. The amount of free VRS in the aqueous phase was determined using high-performance liquid chromatography (HPLC). Formic acid (0.1%)/acetonitrile (70/30) was used as a mobile phase at a flow rate of 1.0 mL/min. VRS was detected at 241 nm. The drug entrapment efficiency and drug loading capacity were calculated using the following equations (Tran et al., 2014a).

$$EE(\%) = (W_{\text{initial drug}} - W_{\text{unbound drug}})/W_{\text{initial drug}} \times 100$$

$$LC(\%) = (W_{\text{initial drug}} - W_{\text{unbound drug}})/W_{\text{lipid}} \times 100$$

where EE is the entrapment efficiency; LC is the drug loading capacity; W is the weight (in mg)

2.5. In vitro release studies

The in vitro release behavior of VRS-SLNs and HA-VRS-SLNs was determined in dissolution medium composed of phosphate buffered saline (pH 7.4) using a dialysis method (Luan et al., 2014; Tran et al., 2014b). 1 mL of formulation was applied in the dialysis bag with a 3500 Da cut-off (Spectra/Por®, CA, USA). The dialysis

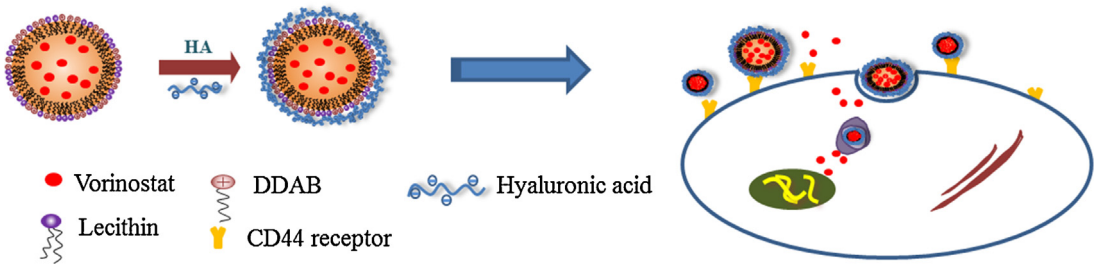

Fig. 1. Diagram illustrating the preparation process for HA-VRS-SLNs.

bag was soaked in a Falcon tube containing 40 mL of dissolution medium. The tube was capped and placed on a shaking water bath (HST–205 SW, Hanbaek ST Co., Korea) at 37 °C with a shaking speed of 100 rpm. The VRS released into the medium at each time point was taken and determined using the HPLC system described above.

2.6. In vitro cytotoxicity studies and cellular uptake

2.6.1. Flow cytometric analysis

Cells (2×10^5 cells/mL) were seeded in each well of a 6-well plate and incubated for 24 h using RPMI 1640 as media. 200 μL of RPMI 1640 (with or without HA at concentration 1 mg/mL) was added for 2 h, and the medium was then discarded and the cells were washed twice with phosphate buffered saline (PBS, pH 7.4). The cells were then treated with NBD-PC-loaded HA-SLNs at a concentration of 1 μg/mL in a humidified incubator with 5% CO_2 atmosphere at 37 °C. After incubation for 30 min, the medium was removed and washed twice with 2 mL of PBS. Cells were then harvested using 0.25% (w/v) trypsin solution then dispersed in 1.5 mL of PBS for flow cytometric measurements using a FACS Calibur flow cytometer (BD Biosciences, San Jose, CA, USA).

2.6.2. Qualitative cellular uptake study by fluorescent microscopy

Cellular uptake of VRS-SLNs and HA-VRS-SLNs was evaluated by confocal microscopy in SCC-7 and MCF-7 cells. In detail, 2×10^5 cells per well were cultured in 12-well plates containing an antiseptic glass coverslip at the bottom of each well and incubated to grow overnight. Cells were continuously treated with 1 μg/mL NBD-PC loaded VRS-SLNs and HA-VRS-SLNs for 30 min, followed by continuous treatment with Lyso-Tracker Red and incubation for 10 min. Cells were then fixed with 4% paraformaldehyde for 15 min after washing three times with PBS. The glass coverslip with the cells was then taken out of the well and placed on a regular glass slide in the presence of mounting agent. Confocal analysis was performed on a Leica TCS SP2 Confocal Microscope (Leica Co., Wetzlar, Germany).

2.6.3. In vitro cytotoxicity studies

Cell-killing activity of VRS-SLNs and HA-VRS-SLNs was measured using the MTT assay with some adjustments (Tran et al., 2014b). 100 μL of cell suspension with 5×10^3 cells/mL were cultured into wells of 96-well test plates and incubated for 24 h at 37 °C in 5% CO_2. A concentration range of blank SLNs, blank HA-SLNs, free VRS, VRS-SLNs, and HA-VRS-SLNs were added to each well-plate, followed by incubation for 24 h. The medium with sample was removed and then washed twice with phosphate-buffered saline. 100 μL MTT solution (1.25 mg/mL MTT in supplemented RPMI medium) was added to the cultures, followed by incubation for 4 h at 37 °C. The obtained formazan crystals were dissolved in 100 μL DMSO. Subsequently, an incubation of 15 min under light protection and at room temperature was performed. The absorbance was measured at 570 nm using a microplate reader (Multiskan EX, Thermo Scientific, Waltham, MA, USA). Cell viability was calculated using the following formula:

$$\text{Cell viability}(\%) = \frac{OD_{570}(\text{sample}) - OD_{570}(\text{blank})}{OD_{570}(\text{control}) - OD_{570}(\text{blank})} \times 100$$

The half-maximal inhibitory concentration (IC_{50}) of each group was calculated using GraphPad Prism 5 software.

2.7. Pharmacokinetics study

2.7.1. Intravenous administration of VRS formulations to rats

Male Sprague-Dawley rats weighing 250 ± 10 g were divided into three groups of four rats. The animals were quarantined in an animal house maintained at 25 ± 2 °C and 50–60% RH, and fasted for 12 h prior to the experiments. The protocols for the animal studies were approved by the Institutional Animal Ethical Committee, Yeungnam University, South Korea.

Three groups of rats received free VRS, VRS-SLNs, and HA-VRS-SLNs by intravenous administration (Tran et al., 2014b). For IV injection of free VRS, VRS was dissolved in PEG 400 and administered at a dose of 10 mg/kg. In case of HA-VRS-SLNs, the lyophilized powder was dissolved in physiological saline (0.9% NaCl) at VRS concentration of 3 mg/mL, accordingly. The pH of solution is 6.4 before injection. Blood samples (300 μL) were collected from the right femoral artery at pre-determined times (0.25, 0.5, 1, 2, 3, 4, 6, 8, 12 and 24 h) after administration of these formulations. The samples were collected in heparin-containing tubes (100 IU/mL) and then immediately centrifuged (Eppendorf, Hauppauge, NY, USA) at 14,000 rpm for 10 min. The plasma supernatant was collected and stored at −20 °C until further analysis.

2.7.2. Plasma sample processing

For extraction of VRS and for precipitation of unwanted protein, 150 μL of plasma was mixed with 150 μL of acetonitrile for 15 min. The samples were then centrifuged at 13,000 rpm for 10 min and 20 μL of the supernatant was injected into the HPLC system for VRS analysis, as described above.

2.7.3. Analysis of pharmacokinetic data

The pharmacokinetic profiles of free VRS, VRS-SLNs, and HA-VRS-SLNs were calculated using the Win-NonLin pharmacokinetic software (v4.0, Pharsight Software, Mountain View, CA, USA). The pharmacokinetic data measured consisting of the area under curves of the plasma drug concentration-time from time zero to infinity ($AUC_{0-\infty}$), the half-life of elimination ($t_{1/2}$), and the mean residence time (MRT) were obtained by summation of the central and tissue compartments. Analysis of variance (ANOVA) was performed to investigate differences between the experimental treatments. A p-value < 0.05 was considered statistically significant in all cases, and all data were expressed as mean ± standard deviation.

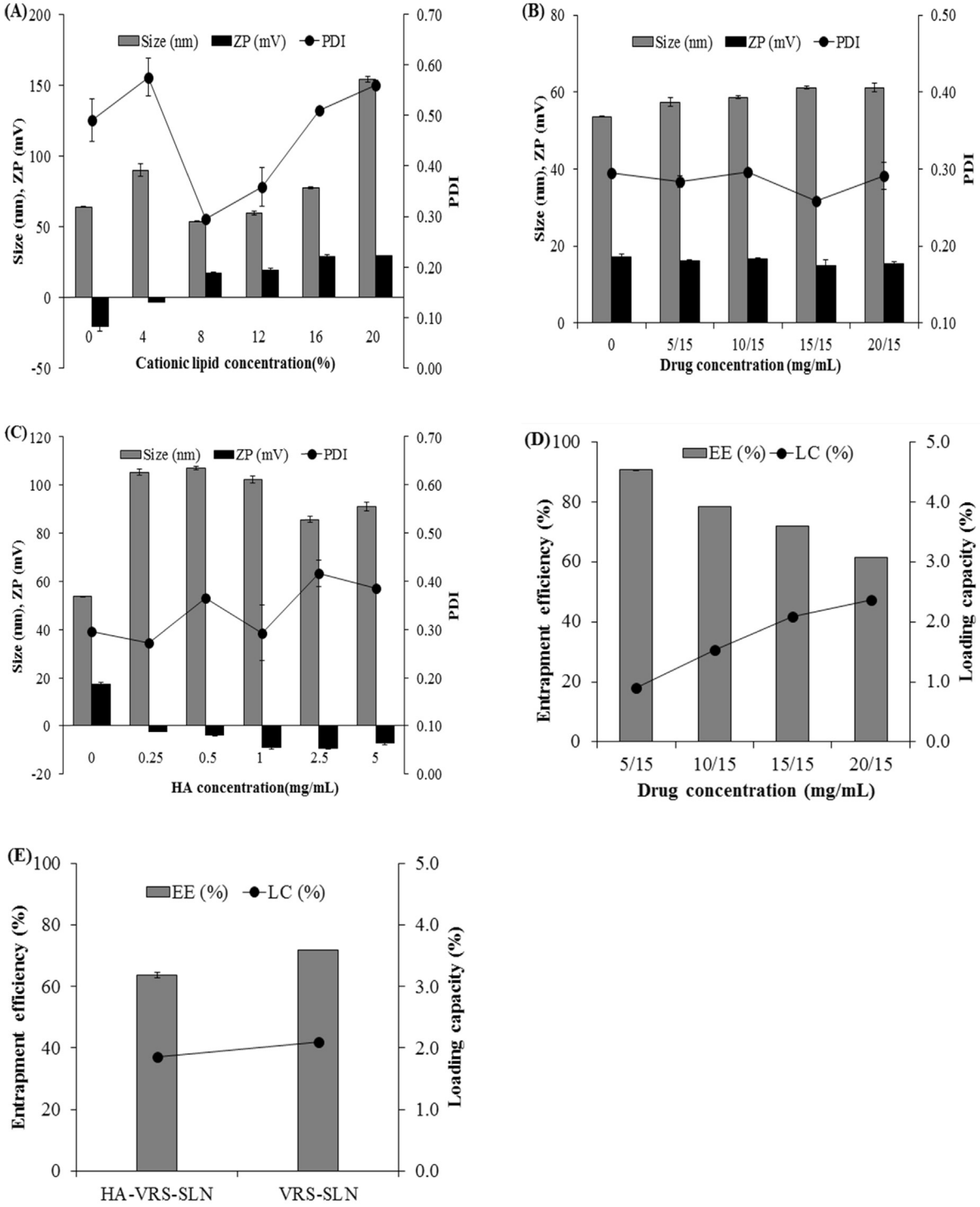

Fig. 2. Effect of (A) Cationic lipid concentration, (B) Drug concentration, (C) HA concentration on formulation parameters: particle size, polydispersity index (PDI), zeta potential (ZP). Effect of (D) drug concentration and (E) HA coating on drug entrapment efficiency and loading capacity. Data are expressed as the mean ± S.D. ($n = 3$).

3. Results and discussion

3.1. Preparation of HA-VRS-SLNs

HA-VRS-SLNs were developed using a cationic solid lipid core and then shedding by anionic polymer, HA (Fig. 1), in order to selectively and preferentially interact with tumor cell surface for effective cancer treatment. As shown in Fig. 1, the core of cationic SLNs was prepared using Compritol as a solid lipid element. Lecithin, DDAB, and Tween 80 were used as helper lipid, cationic lipid, and surfactant, respectively. Fig. 2**A** shows that SLNs were fabricated in particles with average sizes in the range of 50 and 150 nm, and polydispersity index (PDI) of 0.2 and 0.6. Cationic lipid concentration had significant effects on the system, especially PDI and surface charge. Zeta potential measurements determined the surface charge of all particles in aqueous medium in the range

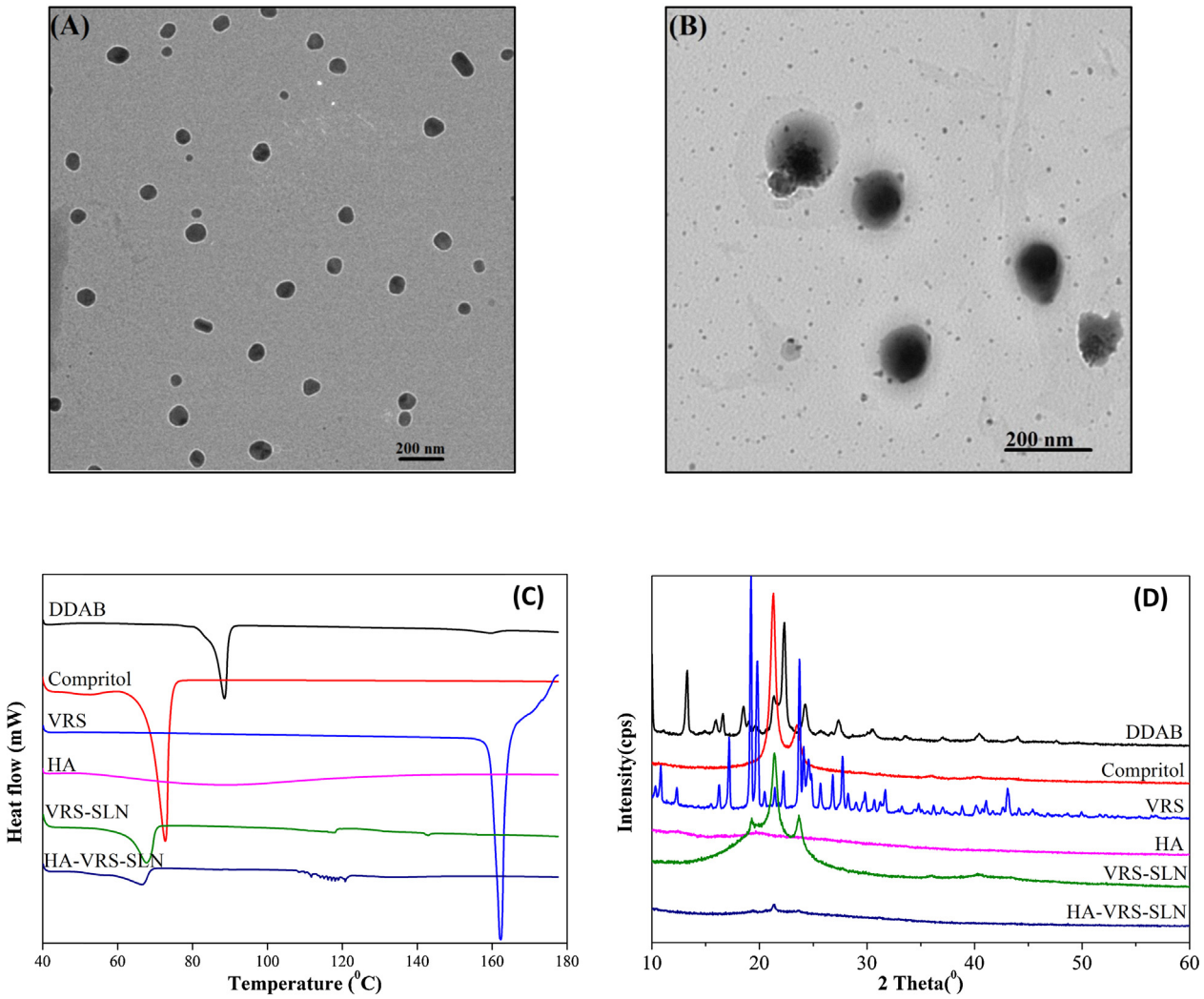

Fig. 3. TEM images of (A) VRS-SLNs and (B) HA-VRS-SLNs. (C) Differential scanning calorimetric thermograms and (D) X-ray diffraction patterns of DDAB, Compritol, free VRS, VRS-SLNs, and HA-VRS-SLNs.

between −20.6 and +29.3 mV. In the presence of 8% DDAB as a cationic lipid, VRS was incorporated into SLNs in order to find the optimal formulation. VRS-loaded SLNs were maintained in terms of size, PDI, and surface charge (Fig. 2**B**). The resulting cationic SLNs were covered with HA via electrostatic interaction. The outer layer of HA dramatically increased particle size and converted the surface charge to a negative charge. When the HA concentration increased, the surface charge also increased, but beyond 1 mg/mL the charge remained constant (Fig. 2**C**). The drug entrapment efficiency and loading capacity demonstrated compatible encapsulation of hydrophobic compound into the lipid core. Upon increase of drug amount, the drug loading capacity was augmented whereas the drug entrapment efficiency was reduced (Fig. 2**D**). This phenomenon is consisted with previous reports (Martins, Sarmento, Nunes, Lúcio, Reis & Ferreira, 2013; Raza, Singh, Singal, Wadhwa & Katare, 2013).

Finally, the formulation, which is composed of 40 mg DDAB as a cationic lipid, 460 mg Compritol, 100 mg Lecithin, 500 mg Tween 80, 15 mg VRS and then coating by 1 mg/mL HA solution was selected for further studies with small size (102.3 ± 1.6 nm), narrow distribution (0.293 ± 0.057), negative charge (−9.0 ± 0.7 mV) and high drug loading (1.86 ± 0.01%). The particles were stored and checked over at least three months, indicating long-term physical stability (data not shown).

3.2. Physical characterization

TEM photomicrographs of the optimized VRS-SLNs and HA-VRS-SLNs are shown in Fig. 3**A** and **3B**. Morphology of both formulations is spherical in shape and well supported by DLS characterization results. Nanoparticles appeared in the range of 60 nm and 110 nm, respectively. In particular, the structure of HA-VRS-SLNs was clearly observed with a black core and transparent shell indicating the HA layer.

DSC and X-ray diffraction were performed for VRS, lipid, HA, VRS-SLNs and HA-VRS-SLNs for characterization of the drug–lipid interactions and the crystallinity of drug before and after formulation in lipid matrices. As shown in Fig. 3**C**, DSC thermogram of bulk compritol, DDAB showed sharp melting peaks at 73 °C and 88 °C, respectively, whereas VRS exhibited a melting peak at 163 °C, corresponding to their natural crystal forms. In contrast, VRS-SLNs and HA-VRS-SLNs did not show the endothermic peak for the VRS around 163 °C. This finding indicates that VRS was in amorphous state or incorporated inside the lipid core (Ramasamy et al., 2014). In addition, sharp peaks were observed for VRS at 2θ-scattered angles of 16.3, 17.2, 19.2, 19.8, 22.2, and 23.7, corresponding to the crystalline nature of the drug, whereas the crystalline state of Compritol was still presented at 2θ-scattered angles of 21.3 and 23.5 (Fig. 3**D**). The intensity of VRS and Compritol peaks was decreased

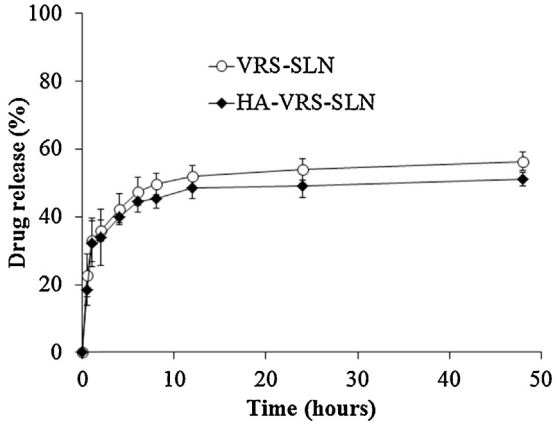

Fig. 4. *In vitro* drug release of VRS from VRS-SLNs (○) and HA-VRS-SLNs (♦) in PBS buffer (pH 7.4, 0.14 M NaCl) at 37 °C. Data are expressed as mean ± S.D. ($n = 3$).

in VRS-SLNs and HA-VRS-SLNs. Less ordered crystal lattices of lipid suggested the successful drug-lipid interaction. In addition, less ordered lipids prevent expulsion of the drug from the particles. Thus, Compritol provides more space for accommodation of drug molecules and limits drug expulsion (Peer, Karp, Hong, Farokhzad, Margalit & Langer, 2007).

3.3. In vitro drug release

In vitro release profiles of VRS from VRS-SLNs and HA-VRS-SLNs formulation were evaluated in pH 7.4 (Fig. 4**)**. The release follows a biphasic profile, characterized by a rapid initial burst (releasing 40% of the drug in 10 h), and followed by a second stage in which few changes were recorded. This two-phase release behavior has been reported for solid lipid nanoparticles (Nabi-Meibodi et al., 2013; Sun, Bi, Chan, Sun, Zhang & Zheng, 2013). The attached drug in the exterior shell and on the particle surface is related to burst release, while the drug that has been encapsulated into the lipid core is released in a sustained manner. This phenomenon was consistent with supposition of drug loading and physical characteristics. On the other hand, HA-VRS-SLNs exhibited a slightly lower release pattern in whole time points. HA layer plays a role as a barrier that could restrict the dispersion of drug to media.

3.4. Intracellular uptake study

Three cell lines present different expression of CD44 receptors (Ghosh, Neslihan Alpay & Klostergaard, 2012; Qhattal & Liu, 2011). To evaluate the intracellular uptake of formulations and the role of CD44 expression on cell surface, the intensity of incorporated dye was visualized and quantified using fluorescence microscopy and flow cytometry (NBD-PC labeled SLNs and HA-SLNs), respectively. Flow cytometry analysis was used to study the cellular uptake efficacy of HA-SLNs with or without pretreated HA. HA-SLNs showed a higher fluorescence shift compared to the controlled group and SLNs in SCC-7 cells, while a few right shifts were observed in the HA-SLNs after pretreatment with HA, indicating less cellular uptake into the SCC-7 cell line (Fig. 5**A**). This phenomenon clearly demonstrates the role of HA-CD44 interaction in terms of enhancing cellular uptake. In contrast, degree of cellular internalization of SLNs into MCF-7 cells after incubation for 30 min was slightly higher than that of HA-SLNs due to possible interaction between positive charge of SLN and negative charge of cell membrane (Fig. 5**B**). This result demonstrates the capacity of HA-SLNs to penetrate high overexpressed CD44 cells (SCC-7) through a process called receptor-mediated endocytosis; meanwhile, there is no significant difference for that system into low overexpressed CD44 cells (MCF-7) (Qhattal & Liu, 2011).

The internalization of SLNs and HA-SLNs was further visualized by confocal laser scanning microscope (CLSM). As shown in Fig. 6, similar results were obtained and agreed with flow cytometry data. In SCC-7 cells, the fluorescence intensity of HA-SLNs was higher than that of SLNs in SCC-7 cells, however, it was reduced by pretreatment with HA, which indicated that surface decoration with HA enhanced cellular uptake of SLNs based on CD44-mediated internalization. In addition, cellular uptake of HA-SLNs in MCF-7 cells was slightly lower than that of SLNs, suggesting that an affinity for CD44 may influence the efficient delivery of payloads.

3.5. In vitro cytotoxicity

The efficacy of the formulations against cancer cells is indicated by their cytotoxicity. Fig. 7 shows cytotoxicity results for cancer cells incubated with five different formulations, including blank HA-SLNs, blank SLNs, free VRS, VRS-SLNs, and HA-VRS-SLNs at 0.5, 1.0, 2.5, 5.0, 12.5, 25.0, and 50.0 μg/ml drug concentrations. Blank HA-SLNs did not show any appreciable cytotoxicity throughout the entire range of concentrations and the cell viability

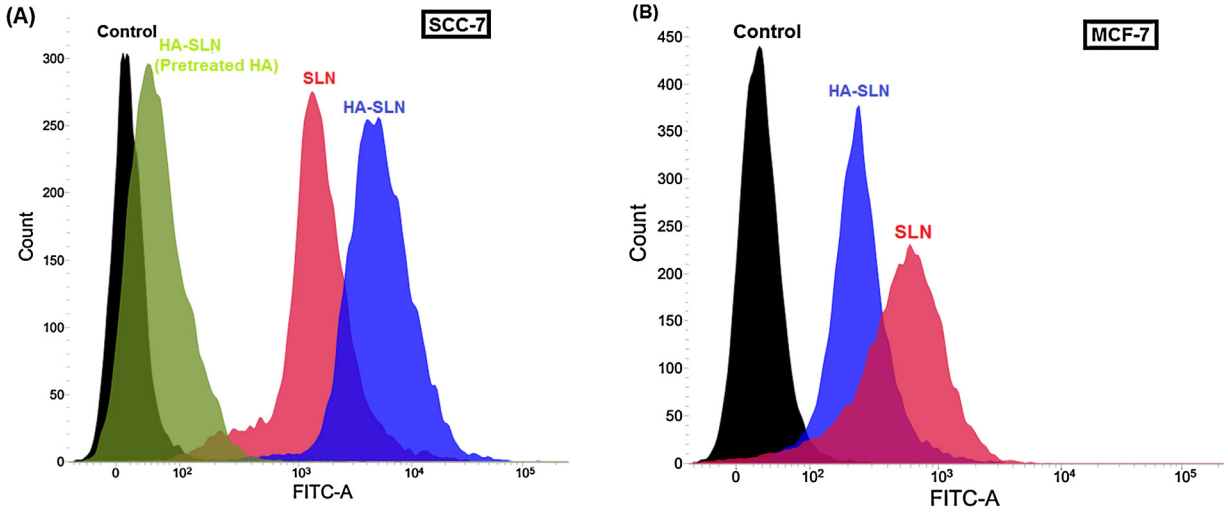

Fig. 5. Quantitative uptake of analysis by flow cytometry of SLNs, HA-SLNs and HA-SLNs pretreated with HA on (A) SCC-7 cells, and (B) MCF-7 cells.

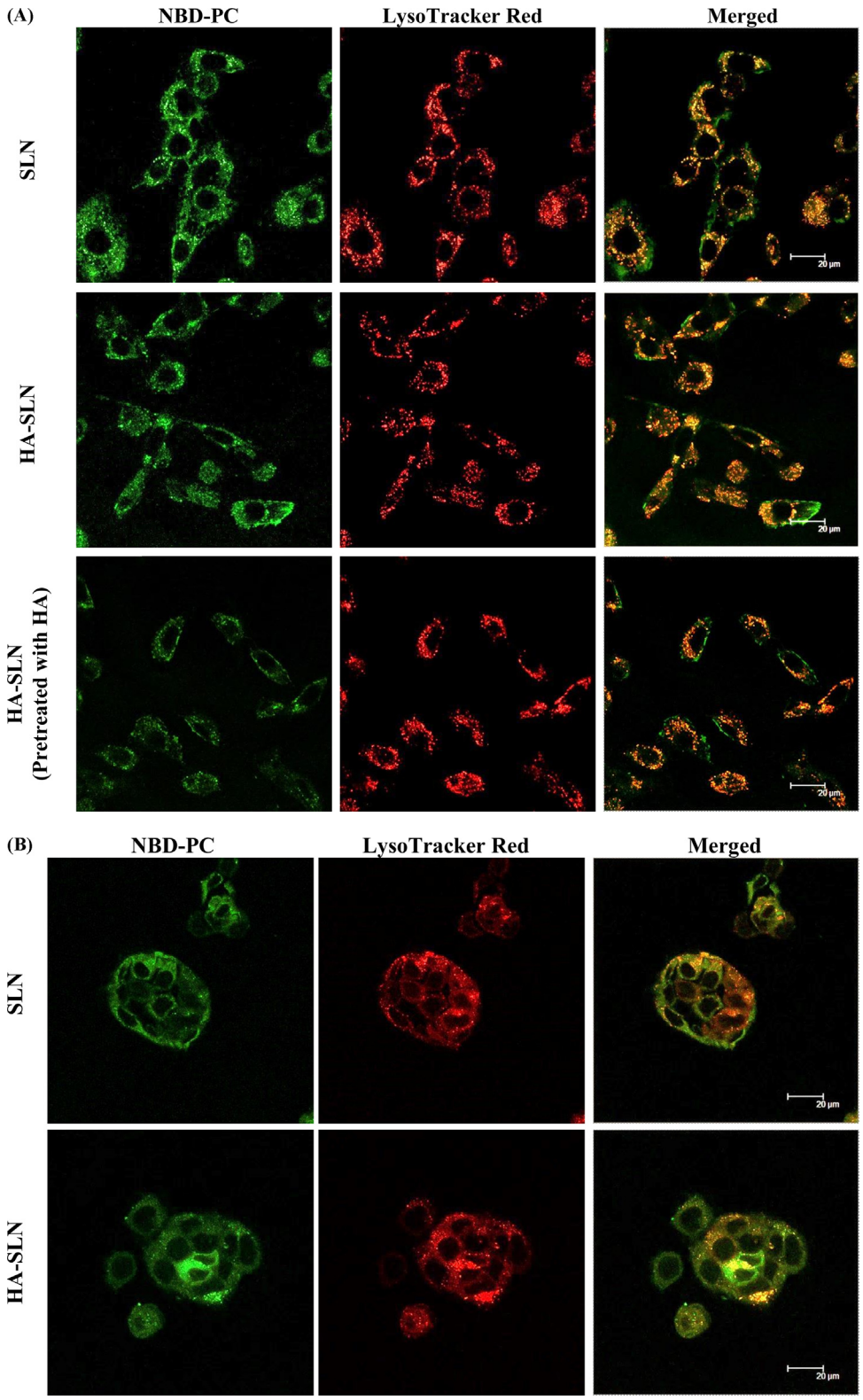

Fig. 6. Intracellular uptake of SLNs and HA-SLNs by confocal laser scan microscope images in (A) SCC-7 cells and (B) MCF-7 cells. SLNs and HA-SLNs containing NBD-PC (green) and Lysotracker Red (red) staining lysosome were used for this experiment. (For interpretation of the references to color in this figure legend, the reader is referred to the web version of this article.).

remained at more than 80% in all cell lines following 24 h exposure, demonstrating its biocompatible nature and tolerance (Petersen, Steiniger, Fischer, Fahr & Bunjes, 2011; Tran et al., 2014a). However, blank SLNs showed a slight cytotoxicity compared with blank HA-SLNs in all cell lines, which could be attributed by cationic DDAB on the surface of SLNs, leading to cell membrane destruction (Yang, Li, Li, Zhang, Feng & Zhang, 2013). In the case of blank HA-SLNs, the outer surface of the lipid was coated with HA so that HA can protect against disruption of cellular membranes, thereby reducing cytotoxicity versus the plain SLN itself. In

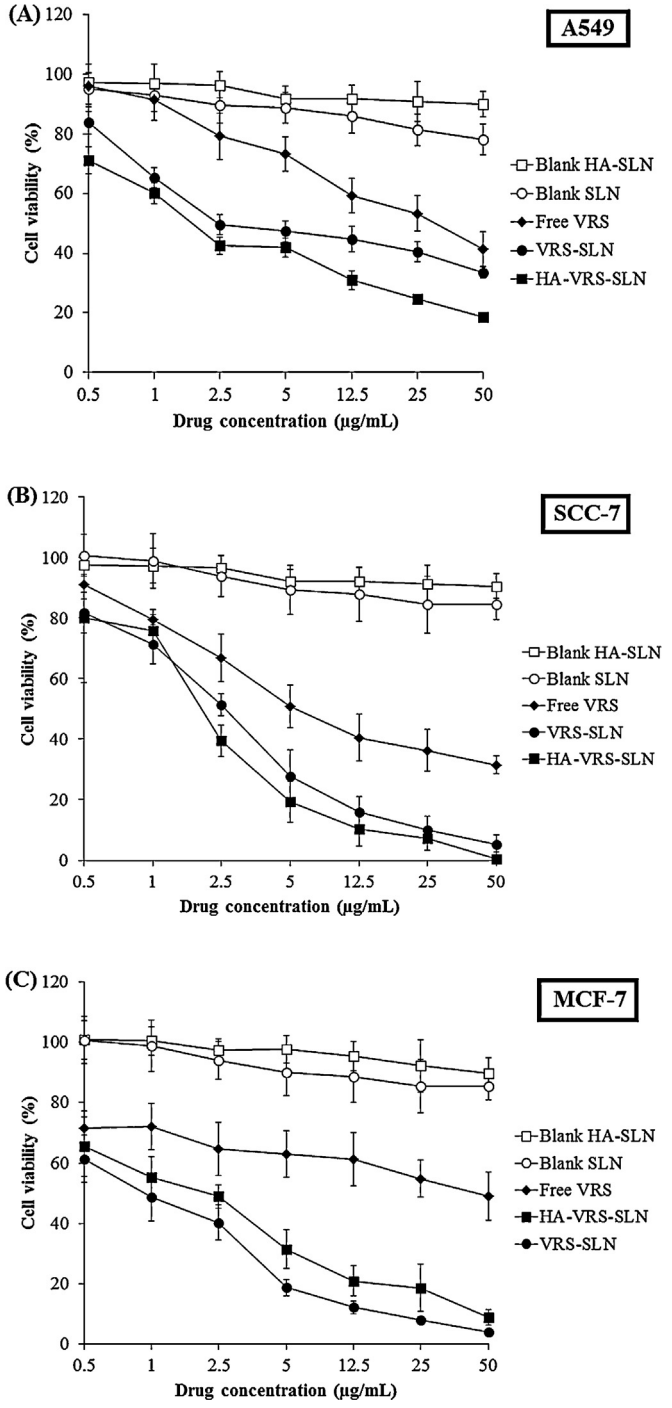

Fig. 7. In vitro cytotoxicity of blank SLNs, blank HA-SLNs, free VRS, VRS-SLNs and HA-VRS-SLNs after 24 h exposure in (A) A549, (B) SCC-7, and (C) MCF-7 cells. Data are expressed as the mean ± S.D. ($n = 8$).

addition, Fig. 7 showed that the cell-killing effects of VRS formulations were concentration-dependent. In all cell lines, in vitro antitumor activity of HA-VRS-SLNs was significantly higher than that of free VRS. The enhanced cytotoxic effect of HA-VRS-SLNs compared to free VRS may reflect the lipophilic nature of the carrier and enhanced intracellular uptake, by a rapid CD44 receptor-mediated endocytosis process (Ramasamy et al., 2013; Tran et al., 2014b). In particular, higher toxicity of HA-VRS-SLNs compared with VRS-SLNs was observed in A549 and SCC-7 cells with a high level of CD44 expression, while HA-VRS-SLNs did not show a better effect than VRS-SLNs MCF-7 cells with low CD44 levels. The good

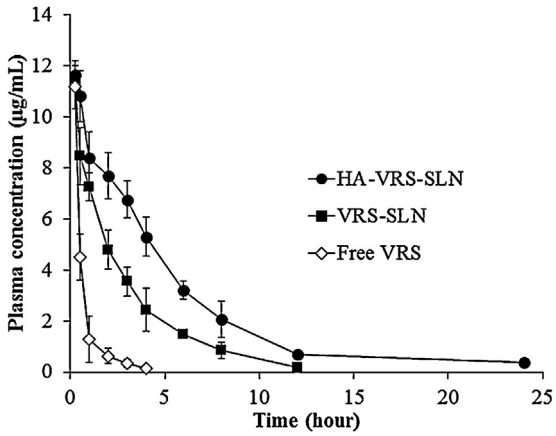

Fig. 8. Plasma concentration-time profile of VRS after intravenous administration at a dose of 10 mg/kg of free VRS (◊), VRS-SLNs (■) and HA-VRS-SLNs (•). Each value represents the mean ± S.D. ($n = 4$).

achievement of HA-VRS-SLNs could also be supposed by charge interaction between positive charge of SLNs and negative surface cell membrane after degradation of HA by HAase (Jiang et al., 2012). This result is consistent with *in vitro* cellular uptake studies by flow cytometric analyses and CLSM. Hence, development of the formulation could improve the therapeutic effect of VRS (Qhattal & Liu, 2011; Wei, Senanayake, Warren & Vinogradov, 2013).

3.6. Pharmacokinetic study

Fig. 8 shows the plasma concentration-time curves of VRS after intravenous administration of free drug suspension, VRS-SLNs and HA-VRS-SLNs. The mean plasma concentrations of VRS after IV injection of HA-VRS-SLNs were higher than those after injection of free VRS and VRS-SLNs. Owing to its hydrophobic property, free VRS was rapidly cleared from the blood stream. Half of VRS was eliminated after 0.65 ± 0.07 h, leading to mean residence time of only 0.77 ± 0.12 h, whereas $t_{1/2}$ and MRT of VRS-SLNs were 2.02 ± 0.52 and 3.20 ± 0.39 h, respectively (Table 1). However, among them, HA-VRS-SLNs showed the best performance with higher plasma concentration, longer half-life and MRT (4.55 ± 0.50, 6.26 ± 0.96 h). With the decrease in *in vivo* clearance, $AUC_{0-\infty}$ values of HA-VRS-SLNs (58.74 ± 6.19 μg.h/mL) were increased significantly ($p < 0.05$), compared with those of free VRS (16.62 ± 1.80 μg.h/mL) and VRS-SLNs (29.81 ± 3.84 μg.h/mL). As shown Fig. 8, VRS-SLNs improved drug state *in vivo*, but it faced clearance by the reticuloendothelial system (RES) due to a positive surface (Dobrovolskaia, Aggarwal, Hall & McNeil, 2008). Coating particles with long circulating agents such as PEG or HA are proposed as a solution to steric stabilization of vesicles and provide protection from opsonization, which is an essential desirable property in drug delivery (Peer, Karp, Hong, Farokhzad, Margalit & Langer, 2007). These results clearly indicated that the HA-coated VRS-SLNs would be successful in causing a reduction in dose and improvement in efficacy of VRS.

Table 1
Pharmacokinetic parameters of VRS in rats after intravenous administration of free VRS, VRS-SLNs, and HA-VRS-SLNs at a dose of 10 mg/kg.

Parameter	Free VRS	VRS-SLNs	HA-VRS-SLNs
C_{max} (μg/mL)	11.17 ± 0.83	11.49 ± 0.11	11.67 ± 0.53
$t_{1/2}$ (h)	0.65 ± 0.07	2.02 ± 0.52[a]	4.55 ± 0.50[a,b]
$AUC_{0-\infty}$ (μg.h/mL)	16.62 ± 1.80	29.81 ± 3.84[a]	58.74 ± 6.19[a,b]
MRT (h)	0.77 ± 0.12	3.20 ± 0.39[a]	6.26 ± 0.96[a,b]

Data are expressed as the mean ± standard deviation ($n = 4$).
[a] $p < 0.05$, compared to the free drug.
[b] $p < 0.05$, compared to VRS-SLNs.

4. Conclusions

In this study, hyaluronic acid was successfully attached onto the surface of cationic SLNs by electrostatic attraction. The resultant particles were spherical in shape, uniform in size with a visually clear outer shell. HA-VRS-SLNs exhibited favorable characteristics that suggested their capability for efficient drug delivery and targeting. First, VRS was released slowly in order to maintain drug concentration in control, leading to reduced toxicity on normal cells. The HA-VRS-SLNs penetrated rapidly into cancer cells, especially on high level CD44 over-expression cells. In addition, the better performance of HA-VRS-SLNs clarified the role of HA in selective targeting to tumor cells. As expected, the HA-VRS-SLNs showed more potency in inhibiting the growth of all cancer cells: A549, SCC7, and MCF-7, compared to that for the VRS and VRS-SLNs. Finally, due to a hydrophilic and negative charge surface, HA-VRS-SLNs stayed longer in blood circulation and prolonged therapeutic drug concentration, which gave the drug a greater chance of reaching the tumor area. Taken together, our data indicated that HA-VRS-SLNs could be successfully developed as a targetable drug delivery system with high bioavailability.

Acknowledgments

This research was supported by the National Research Foundation of Korea (NRF) grant funded by the Ministry of Education, Science and Technology (No. 2012R1A2A2A02044997 and No. 2012R1A1A1039059).

References

Bhushan, S., Kakkar, V., Pal, H. C., Guru, S. K., Kumar, A., Mondhe, D., et al. (2012). Enhanced anticancer potential of encapsulated solid lipid nanoparticles of TPD: A novel triterpenediol from Boswellia serrata. *Molecular Pharmaceutics*, *10*(1), 225–235.

Bolden, J. E., Peart, M. J., & Johnstone, R. W. (2006). Anticancer activities of histone deacetylase inhibitors. *Nature Rreviews Drug Discovery*, *5*(9), 769–784.

Cai, Y., Yap, C., Wang, Z., Ho, P., Chan, S., Ng, K., et al. (2010). Solubilization of vorinostat by cyclodextrins. *Journal of Clinical Pharmacy and Therapeutics*, *35*(5), 521–526.

Choo, Q., Ho, P., & Lin, H. (2008). Histone deacetylase inhibitors: New hope for rheumatoid arthritis? *Current Pharmaceutical Design*, *14*(8), 803–820.

Dobrovolskaia, M. A., Aggarwal, P., Hall, J. B., & McNeil, S. E. (2008). Preclinical studies to understand nanoparticle interaction with the immune system and its potential effects on nanoparticle biodistribution. *Molecular Pharmaceutics*, *5*(4), 487–495.

Ghosh, S. C., Neslihan Alpay, S., & Klostergaard, J. (2012). CD44: A validated target for improved delivery of cancer therapeutics. *Expert Opinion on Therapeutic Targets*, *16*(7), 635–650.

Jiang, T., Zhang, Z., Zhang, Y., Lv, H., Zhou, J., Li, C., et al. (2012). Dual-functional liposomes based on pH-responsive cell-penetrating peptide and hyaluronic acid for tumor-targeted anticancer drug delivery. *Biomaterials*, *33*(36), 9246–9258.

Kelly, W. K., O'Connor, O. A., Krug, L. M., Chiao, J. H., Heaney, M., Curley, T., et al. (2005). Phase I study of an oral histone deacetylase inhibitor, suberoylanilide hydroxamic acid, in patients with advanced cancer. *Journal of Clinical Oncology*, *23*(17), 3923–3931.

Lee, M.-K., Lim, S.-J., & Kim, C.-K. (2007). Preparation, characterization and in vitro cytotoxicity of paclitaxel-loaded sterically stabilized solid lipid nanoparticles. *Biomaterials*, *28*(12), 2137–2146.

Luan, J., Zhang, D., Hao, L., Qi, L., Liu, X., Guo, H., et al. (2014). Preparation, characterization and pharmacokinetics of Amoitone B-loaded long circulating nanostructured lipid carriers. *Colloids and Surfaces B: Biointerfaces*, *114*, 255–260.

Marks, P. A., & Breslow, R. (2007). Dimethyl sulfoxide to vorinostat: development of this histone deacetylase inhibitor as an anticancer drug. *Nature Biotechnology*, *25*(1), 84–90.

Martins, S. M., Sarmento, B., Nunes, C., Lúcio, M., Reis, S., & Ferreira, D. C. (2013). Brain targeting effect of camptothecin-loaded solid lipid nanoparticles in rat after intravenous administration. *European Journal of Pharmaceutics and Biopharmaceutics*, *85*(3, Part A), 488–502.

Mohamed, E. A., Zhao, Y., Meshali, M. M., Remsberg, C. M., Borg, T. M., Foda, M., et al. (2012). Vorinostat with sustained exposure and high solubility in poly (ethylene glycol)-b-poly (dl-lactic acid) micelle nanocarriers: Characterization and effects on pharmacokinetics in rat serum and urine. *Journal of Pharmaceutical Sciences*, *101*(10), 3787–3798.

Nabi-Meibodi, M., Vatanara, A., Najafabadi, A. R., Rouini, M. R., Ramezani, V., Gilani, K., et al. (2013). The effective encapsulation of a hydrophobic lipid-insoluble drug in solid lipid nanoparticles using a modified double emulsion solvent evaporation method. *Colloids and Surfaces B: Biointerfaces*, *112*(0), 408–414.

Peer, D., Karp, J. M., Hong, S., Farokhzad, O. C., Margalit, R., & Langer, R. (2007). Nanocarriers as an emerging platform for cancer therapy. *Nature Nanotechnology*, *2*(12), 751–760.

Petersen, S., Steiniger, F., Fischer, D., Fahr, A., & Bunjes, H. (2011). The physical state of lipid nanoparticles influences their effect on in vitro cell viability. *European Journal of Pharmaceutics and Biopharmaceutics*, *79*(1), 150–161.

Qhattal, H. S. S., & Liu, X. (2011). Characterization of CD44-mediated cancer cell uptake and intracellular distribution of hyaluronan-grafted liposomes. *Molecular Pharmaceutics*, *8*(4), 1233–1246.

Ramasamy, T., Tran, T. H., Cho, H. J., Kim, J. H., Kim, Y. I., Jeon, J. Y., et al. (2013). Chitosan-based polyelectrolyte complexes as potential nanoparticulate carriers: Physicochemical and biological characterization. *Pharmaceutical Research*, 1–13.

Ramasamy, T., Tran, T. H., Choi, J. Y., Cho, H. J., Kim, J. H., Yong, C. S., et al. (2014). Layer-by-layer coated lipid–polymer hybrid nanoparticles designed for use in anticancer drug delivery. *Carbohydrate Polymers*, *102*(0), 653–661.

Raza, K., Singh, B., Singal, P., Wadhwa, S., & Katare, O. P. (2013). Systematically optimized biocompatible isotretinoin-loaded solid lipid nanoparticles (SLNs) for topical treatment of acne. *Colloids and Surfaces B: Biointerfaces*, *105*(0), 67–74.

Rivkin, I., Cohen, K., Koffler, J., Melikhov, D., Peer, D., & Margalit, R. (2010). Paclitaxel-clusters coated with hyaluronan as selective tumor-targeted nanovectors. *Biomaterials*, *31*(27), 7106–7114.

Strobl, J. S., Nikkhah, M., & Agah, M. (2010). Actions of the anti-cancer drug suberoylanilide hydroxamic acid (SAHA) on human breast cancer cytoarchitecture in silicon microstructures. *Biomaterials*, *31*(27), 7043–7050.

Sun, H., Benjaminsen, R. V., Almdal, K., & Andresen, T. L. (2012). Hyaluronic acid immobilized polyacrylamide nanoparticle sensors for CD44 receptor targeting and pH measurement in cells. *Bioconjugate Chemistry*, *23*(11), 2247–2255.

Sun, J., Bi, C., Chan, H. M., Sun, S., Zhang, Q., & Zheng, Y. (2013). Curcumin-loaded solid lipid nanoparticles have prolonged in vitro antitumour activity, cellular uptake and improved in vivo bioavailability. *Colloids and Surfaces B: Biointerfaces*, *111*(0), 367–375.

Tran, T. H., Ramasamy, T., Cho, H. J., Kim, Y. I., Poudel, B. K., Choi, H.-G., et al. (2014). Formulation and optimization of raloxifene-loaded solid lipid nanoparticles to enhance oral bioavailability. *Journal of Nanoscience and Nanotechnology*.

Tran, T. H., Ramasamy, T., Truong, D. H., Shin, B. S., Choi, H.-G., Yong, C. S., et al. (2014). Development of vorinostat-loaded solid lipid nanoparticles to enhance pharmacokinetics and efficacy against multidrug resistant cancer cells. *Pharmaceutical Research*.

Venishetty, V. K., Komuravelli, R., Kuncha, M., Sistla, R., & Diwan, P. V. (2013). Increased brain uptake of docetaxel and ketoconazole loaded folate-grafted solid lipid nanoparticles. *Nanomedicine: Nanotechnology, Biology and Medicine*, *9*(1), 111–121.

Wei, X., Senanayake, T. H., Warren, G., & Vinogradov, S. V. (2013). Hyaluronic acid-based nanogel–drug conjugates with enhanced anticancer activity designed for the targeting of CD44-positive and drug-resistant tumors. *Bioconjugate Chemistry*, *24*(4), 658–668.

Yang, X.-y., Li, Y.-x., Li, M., Zhang, L., Feng, L.-x., & Zhang, N. (2013). Hyaluronic acid-coated nanostructured lipid carriers for targeting paclitaxel to cancer. *Cancer letters*, *334*(2), 338–345.